ELSEVIER

Inorganica Chimica Acta 227 (1994) 269–283

Inorganica Chimica Acta

Synthesis and experimental/theoretical investigation of the high-nuclearity cubic T_d $[Au_6Ni_{12}(CO)_{24}]^{2-}$ cluster, an initial example of a discrete gold–nickel bimetallic-bonded species: comparative analysis of the results of electron-counting methods and the Fenske–Hall MO model in rationalizing the bonding interactions of its Au_6Ni_{12} core consisting of five face-fused metal octahedra ☆

Alison J. Whoolery Johnson [a,1], Brock Spencer [b], Lawrence F. Dahl [a,*]

[a] *Department of Chemistry, University of Wisconsin-Madison, Madison, WI 53706, USA*

[b] *Department of Chemistry, Beloit College, Beloit, WI 53511, USA*

Received 15 July 1994

Abstract

Reactions of the $[Ni_6(CO)_{12}]^{2-}$ dianion with Ph_3PAuCl have led to the isolation and crystallographic/IR/electrochemical characterization of the $[Au_6Ni_{12}(CO)_{24}]^{2-}$ dianion (as the $[PPh_3Me]^+$ salt). Its idealized T_d configuration consists of a central Au_6 octahedron which is tetrahedrally linked to four triangular $Ni_3(CO)_3(\mu_2\text{-}CO)_3$ ligands by the trigonal-antiprismatic (pseudo-octahedral) capping of the four Ni_3 triangles on four alternate Au_6 triangular faces. The resulting structurally unprecedented Au_6Ni_{12} core may be envisioned either as five face-fused octahedra or as the composite of four Au_3Ni_3 octahedra joined by the vertex-sharing of each of the six gold atoms between two adjacent Au_3Ni_3 octahedra. This 18-vertex metal cluster, the first known discrete Au–Ni bimetallic-bonded species, was obtained in low yields (<5%) by the remarkable, unexpected cleavage of the Ph_3P ligand from each gold atom along with concomitant metal–metal condensation to give the Au_6Ni_{12} framework; each $Ni_3(CO)_3(\mu_2\text{-}CO)_3$ fragment retains the pseudo-C_{3v} architecture found in the two $Ni_3(CO)_3(\mu_2\text{-}CO)_3$ moieties comprising the trigonal-antiprismatic $[Ni_6(CO)_{12}]^{2-}$ precursor. A theoretical bonding analysis of the $[Au_6Ni_{12}(CO)_{24}]^{2-}$ dianion was performed via the parameter-free Fenske–Hall MO method in order to elucidate the nature of the Au–Ni orbital bonding interactions. It was found that the π-accepting π^* CO ligands within the four $Ni_3(CO)_3(\mu_2\text{-}CO)_3$ fragments play a crucial role in the formation of this cluster by greatly lowering the energies of the atomic 4p Ni AOs and thereby providing a favorable energy-matching in the orbital overlap of the out-of-plane $4p_z$ Ni AOs with primarily the 6s Au AOs in the central Au_6 octahedron. Four filled, multicenter, two-electron frontier MOs, the a_1 SHOMO (second highest occupied MO) and three t_2 HOMOs under T_d symmetry, provide the essential 'glue' (in addition to presumed relativistic bonding effects due to strongly enhanced 6s–5d gold hybridization) for holding this Au–Ni carbonyl cluster together; each triply degenerate t_2 HOMO (47% Au, 25% Ni, 28% π^* CO) has large 6s Au–$4p_z$ Ni AO bonding interactions, while the totally symmetric a_1 SHOMO (67% Au, 25% Ni, 8% π^* CO) has both 6s Au–6s Au and 6s Au–$4p_z$ Ni AO bonding interactions. In order to reconcile this bonding description obtained from the Fenske–Hall MO method with that obtained from several electron-counting schemes, a qualitative delocalized interoctahedral bonding model is proposed involving four S^σ core-bonding electron pairs for the five face-fused octahedra of this cluster. It is also concluded that this Au_6Ni_{12} cluster furnishes a prime illustration that electron-counting procedures (although generally invaluable in successfully correlating the geometries of small-to-moderately large transition metal clusters to their observed numbers of cluster valence electrons) do not necessarily provide physically meaningful electronic models for the actual bonding in transition metal clusters.

Keywords: Crystal structures; Gold–nickel cluster; Fenske–Hall MO calculation

☆ Dedicated by L.F.D. to Professor György Bor, an exceptional spectroscopist and good friend, on the occasion of his 70th birthday.

* Corresponding author.

[1] Present address: Chemistry Department, St. Cloud State University, St. Cloud, MN 56301-4498, USA.

SSDI 0020-1693(94)04220-P

1. Introduction

A highly active area in cluster chemistry during the last decade has involved the synthesis and characterization of mixed transition metal–gold cluster compounds [1]. Interest in these compounds stems from their potential to serve as models for the particles found in supported gold alloy catalysts [2]. A few of these cluster compounds have also shown catalytic behavior under homogeneous conditions [3]. Incorporation of gold into catalytically active transition metal clusters generally results in an increase in activity and selectivity, even though gold itself is not catalytically active [3d,4]. Similar significant changes in catalytic activity and selectivity have been observed upon addition of gold to platinum heterogeneous catalysts [3b,3c,5].

A number of general synthetic routes for the formation of gold mixed-metal clusters have evolved. Reactions of Ph_3PAuCl with anionic metal carbonyl clusters have given rise to the formation of higher nuclearity clusters in which the $[Ph_3PAu]^+$ moiety occupies edge-bridging or face-bridging sites within the transition metal clusters, often without appreciable alterations of their basic skeletal geometries. A related synthetic route involves reactions of Ph_3PAuMe with neutral metal carbonyl hydride clusters, with the formation of methane serving as the driving force for cluster aggregation. A large number of cationic mixed transition metal–gold clusters have been synthesized by Pignolet and co-workers [3d,6] by reactions of PPh_3AuNO_3 with transition metal phosphine complexes containing Re, Ru, Os, Rh, Ir, Pd and Pt. Gold clusters possessing electron-rich metals have the greatest potential for catalytic activity, given the prominence of these metals in commercial catalysts. In this connection, Pignolet and co-workers [6i,j] recently reported that gold–platinum clusters are very active homogeneous catalysts for the H_2–D_2 equilibration reaction and therefore serve as models for the activation of H_2 by supported Au–Pt catalysts. Teo et al. [7] have synthesized a remarkable series of high-nuclearity gold–silver clusters by reduction of gold and silver salts or complexes with $NaBH_4$ in the presence of tertiary phosphines; these 'supraclusters' or 'clusters of clusters' consist of linear, trigonal and tetrahedral arrangements of vertex-linked centered polyicosahedra, of which the first reported trimetallic supracluster [7j] has a linear $Au_{12}Ag_{12}Pt$ biicosahedral framework composed of two icosahedra, one Pt-centered and one Au-centered, sharing a common Au atom. Steggerda and co-workers [7k] subsequently reported a structurally analogous $Au_{10}Ag_{13}Pt_2$ biicosahedral supracluster consisting of two identical Pt-centered icosahedral subunits sharing a common Ag vertex.

While large numbers of gold–metal clusters containing eight of the nine electron-rich Group VIII (8–10) transition metals (viz., Fe, Ru, Os, Co, Rh, Ir, Pd, Pt) have been isolated, it is curious that prior to this research there were no reports in the literature of gold–nickel bimetallic-bonded compounds. Consequently, our efforts were directed towards the synthesis of a gold–nickel cluster by reaction of the $[Ni_6(CO)_{12}]^{2-}$ dianion with Ph_3PAuCl. It was hoped that the trigonal faces of the trigonal-antiprismatic (pseudo-octahedral) $[Ni_6(CO)_{12}]^{2-}$ dianion would serve as viable sites for the coordination of $[AuPPh_3]^+$ fragments. No such cluster adduct was isolated. Rather, in addition to small amounts of the known $Au_{11}(PPh_3)_7Cl_3$ cluster [8], a new gold–nickel cluster, $[Au_6Ni_{12}(CO)_{24}]^{2-}$, was isolated in low yield. This cluster is formed via bond-scission of the PPh_3 ligand in the precursor from the gold atom, resulting in a central octahedron of gold atoms which is capped on each of four alternating faces by a triangular $Ni_3(CO)_3(\mu_2\text{-}CO)_3$ ligand in a trigonal-antiprismatic (pseudo-octahedral) configuration. The cleavage of the PPh_3 ligand from each gold atom was unexpected, because the PPh_3 ligand in Ph_3PAuCl is generally retained by the gold atom in other cluster aggregation reactions.

Attempts to isolate and characterize other gold–nickel clusters were unsuccessful. Reaction products were highly susceptible to decomposition within short periods of time, even when kept under inert atmosphere, indicating that these products were quite unstable. The apparent instability of gold–nickel systems in general, as evidenced by the absence of gold–nickel clusters in the literature, prompted us to investigate the bonding in the geometrically-unprecedented $[Au_6Ni_{12}(CO)_{24}]^{2-}$ dianion by use of the Fenske–Hall molecular orbital method [9]. It was hoped that this theoretical investigation would provide a definitive understanding of the nature of the Au–Ni bonding interactions which not only would account for the occurrence of this unique gold–nickel cluster but would also furnish insight concerning the possible designed synthesis of other stable gold–nickel clusters. The calculated orbital components of the four frontier MOs obtained via the Fenske–Hall MO model for this cluster are shown to conform to a multicenter core-bonding description involving five face-fused metal octahedra. In striking contrast, it is also shown herein that the normal application of different electron-counting methods [11–13] predicts the correct valence electron total for four vertex-sharing Au_3Ni_3 octahedra but *not* for five face-fused metal octahedra (i.e. the central Au_6 octahedron is assumed not to contain a multicenter core bond). A qualitative delocalized interoctahedral bonding model is proposed to resolve this problem by modification of two valence electron-counting schemes such that the predicted cluster valence electron count for five face-fused octahedra agrees with the observed electron count. It is our current premise (vide infra) that this comparative analysis provides a striking illustration that

qualitative electron-counting procedures do not necessarily provide a physically meaningful description of the actual electron-density bonding interactions in transition-metal cluster systems. A preliminary account of the synthesis and structural analysis of this cluster has been reported [10].

2. Experimental

2.1. General comments

All reactions and manipulations were carried out under an inert atmosphere of dry nitrogen gas using standard Schlenk apparatus or a nitrogen-filled Inert Atmospheres glove box. All solvents were dried and distilled under nitrogen immediately prior to use. The following drying agents were used: hexane (CaH_2), toluene (Na), THF (K/benzophenone), diisopropyl ether (K/benzophenone), acetone ($CaCO_3$), and methanol (Mg).

The $[Ni_6(CO)_{12}]^{2-}$ dianion [14] as the Na^+ salt was prepared by use of a slightly modified version of the synthesis published by Longoni et al. [14b]. This Na^+ salt was then metathesized to the $[PPh_3PMe]^+$ salt by addition of $[PPh_3Me]^+Br^-$ (Aldrich). Ph_3PAuCl was prepared [15] from $HAuCl_4$ (AESAR/Johnson Matthey). SiO_2 (Kieselgel 60, 230–400 mesh: Merck) was activated by heating it to 180 °C for 24 h, followed by addition of 5% H_2O by weight to ensure consistent activity.

IR spectra were obtained with a Beckman model IR-4240 spectrophotometer using nitrogen-purged solution cells with CaF_2 windows. Cyclic voltammograms were obtained with a Bioanalytical Systems electrochemical analyzer (BAS-100); these experiments were performed with a Princeton Applied Research (PAR) electrochemical cell in a nitrogen-filled Vacuum Atmospheres drybox. The cell consisted of a platinum disk working electrode and a coiled platinum wire counter electrode. The reference electrode was a porous Vycor-tipped aqueous saturated calomel electrode separated from the test solution by a salt bridge with a 0.1 M tetra-n-butylammonium hexafluorophosphate/MeCN filling solution. Additional details are given elsewhere [16]. An *iR* compensation for solution resistance [17] was made before determination of the current versus voltage curves.

2.2. Preparation of the $[Au_6Ni_{12}(CO)_{24}]^{2-}$ dianion

In a typical reaction, $AuPPh_3Cl$ (0.30 g, 0.60 mmol) was dissolved in 20 ml of THF and added dropwise via a stainless steel cannula to a stirred suspension of $[PPh_3Me]^+_2[Ni_6(CO)_{12}]^{2-}$ in 70 ml of THF. The mixture immediately changed from a bright orange–red to a dark red color with concomitant formation of a dark brown precipitate. After being stirred under anaerobic conditions at room temperature for 18 h, the red solution was filtered from the brown solid. Addition of hexane to the red solution resulted in complete precipitation of the mixture. It should be noted that this reaction mixture is highly unstable and is very susceptible to decomposition when solvent is removed by N_2 purge or under vacuum. The solid was washed with hexane, then redissolved in 15 ml of THF and chromatographed under N_2 on an SiO_2 gel column. Elution produced three separate bands. The first band eluted with THF was peach colored; an IR spectrum of this band in THF displayed only carbonyl frequencies in the terminal carbonyl region. Efforts to crystallize this band were unsuccessful. The second band eluted with THF was bright red in color and quite unstable; an IR spectrum of this band contained bands in both the terminal and bridging carbonyl regions. Efforts to crystallize this band were unsuccessful due to excessive decomposition of the material. The third band eluted with 95% THF/5% acetone gave the title compound which was crystallized as the $[PPh_3Me]^+$ salt by slow diffusion of diisopropyl ether into a concentrated THF solution.

The brown precipitate which was observed in the reaction flask was extracted with acetone. An IR spectrum (in acetonitrile) showed broad absorptions at 1993(s) and 1888(s) cm^{-1}. Two contrasting sets of crystals of different morphology and color (viz. red and black) were obtained by slow diffusion of diisopropyl ether into an acetone solution. X-ray diffraction studies of one red plate-like crystal revealed the compound to be the known $Au_{11}(PPh_3)_7Cl_3$ [8]. Most of the crystals were black in color; none was suitable for X-ray diffraction studies.

2.3. Characterization of $[PPh_3Me]^+_2[Au_6Ni_{12}(CO)_{24}]^{2-}$

Dark red in color, this compound is moderately unstable to air, both in the solid state and in solution. It is insoluble in non-polar solvents such as hexane, benzene and toluene but soluble in THF, acetone and acetonitrile. An IR spectrum in THF solution exhibits carbonyl frequencies at 2040(s), 1860(s) and 1840(m) cm^{-1}. A cyclic voltammogram in acetonitrile displayed a quasi-reversible reduction wave at $E_{1/2} = -1.5$ V (versus SCE) and an irreversible oxidation wave at $E_p = +1.4$ V.

2.4. Structural determination of $[PPh_3Me]^+_2[Au_6Ni_{12}(CO)_{24}]^{2-} \cdot C_4H_8O$

A block-like black crystal with dimensions $0.5 \times 0.5 \times 0.5$ mm was glued with epoxy inside an argon-filled 1.0 mm Lindemann glass capillary. The ortho-

rhombic crystal structure was determined from single-crystal X-ray data collected on a Siemens P3F diffractometer with graphite-monochromated Mo Kα radiation ($\lambda = 0.71073$ Å). Cell dimensions and the orthorhombic D_{2h}-*mmm* Laue symmetry were verified from axial photographs. The data were corrected for Lorentz and polarization effects and for a small crystal-decay (i.e. ~3%, based on three standard reflections monitored every 47 reflections during data collection). Measured intensities of one independent reciprocal-lattice octant gave 14 113 data, of which 7656 independent reflections (with $|F| \geq 3.0\sigma(F)$) were utilized in the refinement. An empirical psi-scan absorption correction based on 360 psi-scan measurements was made [18]. The structure was elucidated via direct methods followed by successive Fourier difference maps which revealed the independent atomic positions of one dianion, two $[PPh_3Me]^+$ counterions, and a THF solvent molecule. For least-squares refinement, each of the six phenyl rings was constrained as a rigid group (idealized to the well-known D_{6h} geometry of the benzene ring). All non-hydrogen atoms were refined anisotropically except the phenyl ring carbon and THF atoms which were refined isotropically. The phenyl hydrogen atoms were included as fixed-atomic isotropic contributors ($U = 0.08$ Å^2) with idealized coordinates during the final stages of refinement. A final difference map exhibited no unusual features. The largest positive residual peaks were heavy-atom ripples located at physically non-meaningfull distances (i.e. too short to be due to light atoms) from the Au_6 octahedron. The absence at the center of the Au_6 octahedron of a significant electron-density peak, the assigned isotropic thermal parameter of which upon an arbitrary designation as an interstitial carbon atom 'blew up' to an abnormally high value upon a separate least-squares refinement, provided convincing evidence for a non-centered Au_6 octahedron (vide infra).

Crystal data, data collection and refinement parameters are presented in Table 1. Atomic positional parameters and equivalent isotropic thermal parameters, selected interatomic distances, bond angles, anisotropic thermal parameters, and idealized coordinates for the hydrogen atoms are available elsewhere [10,19].

Table 1
Crystal, data-collection, and refinement parameters for $[PPh_3Me]^+{}_2[Au_6Ni_{12}(CO)_{24}]^{2-} \cdot C_4H_8O$

Temperature (°C)	18
Formula	$Au_6Ni_{12}P_2C_{66}O_{25}H_{44}$
Formula weight (g mol^{-1})	3185.22
$F(000)$	10224
Crystal system	orthorhombic
a (Å)	17.730(5)
b (Å)	29.518(6)
c (Å)	30.676(14)
V (Å^3)	16054.4(93)
Space group	*Pbca*
Z	8
D_x (calc.) (g cm^{-3})	2.64
μ (mm^{-1})	7.21
Scan mode	Wyckoff ω
2θ limits (°)	3.5–50
Scan speed (°/min)	variable (2.93–29.3)
No. check reflections/data	3/47
No. independent data ($\|F\| > 3\sigma(F)$)	7657
No. parameters refined	708
Data/parameter ratio	10.8:1
$R(F)$ [a]	8.38
$R_w(F)$ [a]	7.74
Goodness-of-fit (GOF) [a]	1.29

[a] $R(F) = \Sigma\|F_o| - |F_c\|/\Sigma|F_o| \times 100$; $R_w(F) = [\Sigma w_i\|F_o| - |F_c\|^2/\Sigma w_i|F_o|^2]^{1/2} \times 100$; GOF $= [\Sigma w_i\|F_o| - |F_c\|^2/(m-n)]^{1/2}$, where $w_i = [\sigma^2(F_o) + (0.0009)F_o^2]^{-1}$; m = no. independent data, and n = no. variable parameters.

2.5. Fenske–Hall molecular orbital calculations of the $[Au_6Ni_{12}(CO)_{24}]^{2-}$ dianion

2.5.1. General comments

Molecular orbital calculations were done with the Fenske–Hall model on a Micro Vax II computer system [19]. This MO model is based on a non-parameterized, non-empirical, approximate Hartree–Fock–Roothaan procedure. The results of each calculation (eigenvectors and eigenvalues) are completely determined by the nature and size of the basis set and by the assumed geometry of the molecule. A detailed description of this method and examples of its applications are given elsewhere [20–23].

2.5.2. Basis functions

Basis functions for neutral C, O and Au atoms and for monocationic Ni atoms contained in the Fenske–Hall molecular orbital package were originally generated by the numerical Xα atomic orbital program of Herman and Skillman [24] in conjunction with the Xα-to-Slater basis program of Bursten and Fenske [25]. These basis functions are based upon ground-state atomic configurations for carbon and oxygen and a $d^{10}s^1$ neutral configuration for each gold atom. Each nickel atom was assumed to possess a d^9s^0 cationic configuration; the valence s and p exponents for the nickel atoms were determined by minimizing the energy difference between the valence eigenvalues obtained from molecular calculations and the experimental ionization potentials of $Ni(PF_3)_4$ [20]. The numerical Xα-AOs were fit to double-ζ analytical Slater-type functions for the valence d AOs of the Ni and Au atoms.

2.5.3. Geometry

The geometry for $[Au_6Ni_{12}(CO)_{24}]^{2-}$ was taken from the X-ray structural data for $[PPh_3Me]^+{}_2$-$[Au_6Ni_{12}(CO)_{24}]^{2-} \cdot C_4H_8O$ and idealized to T_d symmetry based upon the average bond distances given in Table 2.

Table 2
Bond lengths (Å) used in the idealized geometry of $[Au_6Ni_{12}(CO)_{24}]^{2-}$ (1) [a]

Au–Au	2.835	Ni–C_T	1.780
Au–Ni	2.694	Ni–C_B	1.913
Ni–Ni	2.400	C_T–O_T	1.110
		C_B–O_B	1.160

[a] Subscripts T and B denote terminal and bridging carbonyl ligands, respectively.

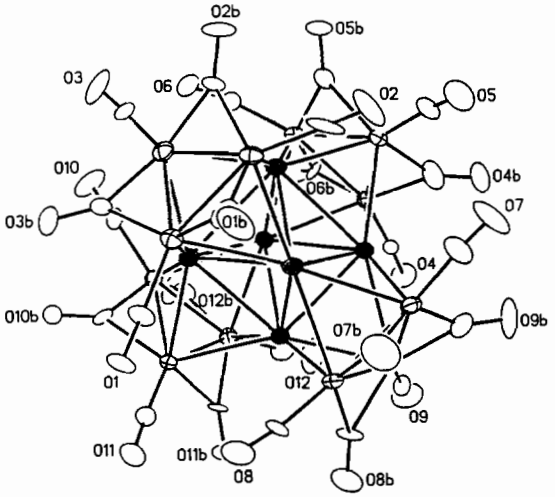

Fig. 1. $[Au_6Ni_{12}(CO)_{24}]^{2-}$ dianion with atomic thermal ellipsoids of 20% probability.

3. Results and discussion

3.1. Description of the structure of $[PPh_3Me]^+{}_2[Au_6Ni_{12}(CO)_{24}]^{2-}\cdot C_4H_8O$

The orthorhombic cell of *Pbca* symmetry contains 8 discrete dianions, 16 cations, and 8 tetrahydrofuran solvent molecules, all located in general positions. There are no interionic contacts shorter than normal van der Waals separations.

The idealized T_d configuration of the $[Au_6Ni_{12}(CO)_{24}]^{2-}$ dianion (**1**), shown in Fig. 1, consists of a central Au_6 octahedron which is capped on each of four alternate faces by an $Ni_3(CO)_3(\mu_2\text{-}CO)_3$ ligand oriented in a trigonal-antiprismatic (pseudo-octahedral) configuration. The Au_6Ni_{12} core (Fig. 2) can be described either as five face-fused octahedra or as a composite of four vertex-sharing Au_3Ni_3 octahedra. Each of the four equilateral nickel triangles contains an analogous arrangement of three terminal and three doubly bridging carbonyl ligands, as found in the two $Ni_3(CO)_3(\mu_2\text{-}CO)_3$ moieties comprising the trigonal-antiprismatic $[Ni_6(CO)_{12}]^{2-}$ precursor.

The 12 independent Au–Au distances in the central Au_6 octahedron of **1** vary from 2.786(2) to 2.882(2) Å; the mean of 2.84 Å is shorter than the corresponding

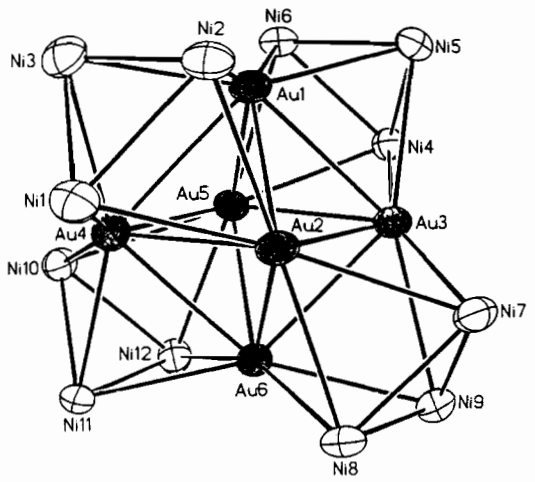

Fig. 2. T_d Au_6Ni_{12} core of the $[Au_6Ni_{12}(CO)_{24}]^{2-}$ dianion (**1**) with atomic thermal ellipsoids of 35% probability.

mean Au–Au distance of 2.98 Å on the 'surfaces' of the $Au_{11}X_3(PAr_3)_7$ clusters (where X = I, SCN, CN; Ar = *p*-YC_6H_4 in which Y = Cl, F, Me) [26] but comparable to the mean Au–Au distance of 2.81 Å on the 'surface' of the $[Au_9(P\{p\text{-tol}\}_3)_8]^{3+}$ cluster (where *p*-tol denotes 4-methylphenyl) [27]. To our knowledge, there are no previous examples of a non-centered octahedral Au_6 cluster. The yellow $[Au_6(P\{p\text{-tol}\}_3)_6]^{2+}$ dication, originally formulated [28] as a non-centered octahedral cluster, was recently shown by Schmidbaur and co-workers [29] from their extensive work on the analogous $[Au_6(PPh_3)_6(\mu_6\text{-C})]^{2+}$ dication to be the corresponding $[Au_6(P\{p\text{-tol}\}_3)_6(\mu_6\text{-C})]^{2+}$ dication with octahedral coordination of the six $AuPR_3$ fragments to an interstitial carbon atom; the presence of the carbide-centered atom in this $Au_6(\mu_6\text{-C})$ cluster gives rise to a normal electron count [30] and accounts for the significantly longer Au–Au distances of 3.02 Å (av.). Of particular relevance is that both non-relativistic and relativistic theoretical analyses [31,32] of these $[Au_6(PR_3)_6(\mu_6\text{-C})]^{2+}$ dications suggest attractive tangential interactions between the Au(I) atoms with Au–Au distances of 3.0 Å; these conclusions are in accordance with spectroscopic/crystallographic evidence by Schmidbaur and co-workers [33] for the existence of attractive tangential interactions between Au(I) atoms in these and other gold compounds. The 0.2 Å shorter Au–Au distances in **1** indicate relatively strong direct Au–Au bonding within the non-centered gold octahedron.

The possibility that the Au_6 octahedron in **1** also has a second-row interstitial atom at its center was ruled out on account of the observed absence in the final difference map of a significant electron-density residual peak (whose assigned isotropic thermal parameter upon an arbitrary designation as a carbon atom 'blew up' in a least-squares refinement). The non-existence of an interstitial atom such as carbon is likewise

consistent with the octahedral Au_6 cavity in **1** being too small to accommodate a carbon-centered atom, as evidenced by its mean Au–Au edge-contact distance being substantially shorter (by 0.2 Å) than that in the reformulated $[Au_6(P\{p\text{-tol}\}_3)_6(\mu_6\text{-C})]^{2+}$ (3.02 Å) as the $[BPh_4]^-$ salt [28], in $[Au_6(PPh_3)_6(\mu_6\text{-C})]^{2+}$ (3.00 Å) as the $[MeOBF_3]^-$ salt [29], and in $[Au_6(P\{i\text{-Pr}\}_3)_6(\mu_6\text{-C})]^{2+}$ (3.02, 3.03 Å for two independent half-cluster dications) as the $[B_3O_3F_4]^-$ salt [33c]. In addition, the Fenske–Hall MO results and electron-counting models presented herein (vide infra) provide convincing support for both the composition and structure of **1**.

The 24 independent Au–Ni distances in **1** vary from 2.632(4) to 2.757(4) Å with a mean of 2.69 Å. Although no Au–Ni bond distances have been reported previously, comparison to reported Au–Co bond distances (which range from 2.46 to 2.87 Å and are typically between 2.65 and 2.75 Å) [34] and to the only reported Au–Cu bond distance of 2.896 Å [35] indicates that the 2.69 Å distance in **1** is also consistent with strongly bonding Au–Ni interactions. The average distance of 2.40 Å for the 12 intratriangular carbonyl-bridged Ni–Ni distances (2.385(6)–2.410(5) Å range) in **1** is virtually identical to the average Ni–Ni distance for the corresponding $Ni_3(CO)_3(\mu_2\text{-CO})_3$ fragments contained in the $[Ni_6(CO)_{12}]^{2-}$ dianion (2.38 Å) [14a], in the $[Ni_9(CO)_{18}]^{2-}$ dianion (2.39 Å) [36], and in the $[Ni_{12}(CO)_{21}H_{4-n}]^{n-}$ anions ($n=2$–4) [37]. The mean terminal and doubly bridging Ni–CO distances are 1.78 and 1.91 Å, respectively, while the mean terminal and doubly bridging C–O distances are 1.11 and 1.16 Å, respectively. The terminal carbonyl ligands lie essentially in the plane of the Ni_3 triangle, whereas the bridging carbonyls are tilted by 24° (av.) out of the plane of each nickel triangle away from the Au_6 octahedron.

3.2. Molecular orbital analysis

3.2.1. General considerations

The origin of the right-handed master coordinate system was chosen to be at the center of the gold octahedron. Right-handed local coordinate systems were defined as follows: the z axis of each of the gold atoms points at the origin of the master coordinate system, the z axis of each nickel atom is perpendicular to the plane containing the nickel triangle, and the z axis of each carbon atom points toward the oxygen and vice versa for the z axis of each oxygen atom in each carbonyl ligand.

The cluster was divided into five fragments: four neutral $Ni_3(CO)_3(\mu_2\text{-CO})_3$ triangles and the neutral gold octahedron. Calculations were first carried out on these fragments and then on the composite $Au_6Ni_{12}(CO)_{24}$ cluster. The eigenvectors resulting from calculations of the Au_6 octahedron and the $Ni_3(CO)_3(\mu_2\text{-CO})_3$ fragments were used as basis sets when the calculation was done on the entire molecule. This transformation of the basis sets from atomic orbitals to molecular 'fragment' orbitals allows for an easier interpretation of the Ni–Au bonding scheme in the molecular complex. In order to simplify the fragment analysis, calculations were performed initially on the 'hypothetical' neutral cluster transformed from the neutral fragments, after which the two additional electrons corresponding to the negative charge were added. Subsequent calculations for the cluster dianion showed little change in orbital compositions and relative orbital energies of the frontier MOs compared to the corresponding ones for the hypothetical neutral cluster, although all frontier MOs in the dianion were expectedly shifted to higher energies by an approximately constant factor.

3.2.2. Fragment analysis

(*i*) *Au_6 octahedron.* The qualitative conclusions of this MO calculation on the neutral Au_6 octahedron support those of a previous extended-Hückel treatment [30a]. The filled gold 5d AOs combine to form a narrow band of 30 Au_6 symmetry orbitals (SOs) at low energies. The d–d overlap integrals are small to the point of being almost insignificant, causing the energy-spread of the SOs generated to be rather small when these AOs combine in an Au_6 cluster. This feature is characteristic of the late transition elements and arises primarily from a radial contraction of the d AOs due to insufficient screening effects as the nuclear charge increases across a given row of the transition metal series. At higher energies there are six SOs with predominately gold 6s character, and, at higher energies still, 18 SOs with predominately gold 6p character. The most important frontier orbitals to be considered are the filled a_{1g} and t_{1u} SOs (under O_h symmetry) depicted in Fig. 3. The filled a_{1g} SO is composed of the totally symmetric combination of the gold 6s AOs and is strongly metal–metal bonding. The partially filled triply degenerate t_{1u} SOs consist of essentially non-bonding combinations of *trans* 6s orbitals (with some mixing of the higher-lying $6p_x$ and $6p_y$ orbitals). The energies and percent compositions of the important frontier SOs for this Au_6 fragment are given in Table 3.

The Fenske–Hall model does not take into account relativistic effects associated with the heavy gold atoms [31,38–41]. The extremely large relativistic core effect for the gold atom manifests itself in increasing its relative electronegativity and substantially altering the chemical and spectroscopic properties of gold-containing compounds. In Au(I) complexes the relativistic contraction of the outer valence 6s Au AO (by ~17%) and concomitant relativistic expansion of the 5d Au AOs induces 6s–5d hybridization and thereby gives rise to greater stability and shorter Au–Au and Au–ligand bonds in gold clusters [31,39–41].

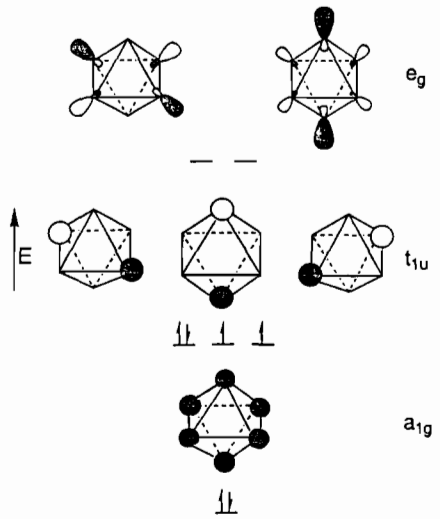

Fig. 3. Frontier molecular orbitals for the neutral Au_6 octahedron. Symmetry labels are for an idealized O_h geometry.

Table 3
Energies and percent compositions of the frontier molecular orbitals for the neutral Au_6 octahedron under O_h symmetry

MO	Energy (eV)	6s (%)	$6p_z$ (%)	$6p_x$,$6p_y$ (%)
a_{1g} (SHOMO)	−6.37	100		
t_{1u} (HOMOs)	−3.23	75.3	3.7	15.4
e_{1g} (LUMOs)	−1.93	67.5	31.6	

In conjunction with spectroscopic studies [42d,42e] of Au_6^- and the extensive physical/chemical characterization of the $[Au_6(PR_3)_6(\mu_6\text{-}C)]^{2+}$ dications [29,33], sophisticated ab initio theoretical treatments including relativistic effects have been carried out on naked Au_6^n species ($n=2+$, $1+$, 0, $1-$) [31,42a–42c] and on hypothetical $[Au_6X]^n$ cores (X=B, Al, $n=1+$; X=C, Si, $n=2+$; X=N, P, $n=3+$) containing an interstitial X atom encapsulated in an Au_6 octahedron [41b]. Of interest is that a capped pentagonal geometry (C_{5v}) with an $^1A_1$ ground state was found at the highest level of theory [42a,42b] to be the most favorable structure in energy for neutral Au_6; the lowest energy state of the Au_6^+ ion was found to be a $^2E_1$ state with the capped pentagonal structure, and hence this state was predicted to undergo a Jahn–Teller distortion [42a].

Scattered-wave Xα calculations performed [31,42c] for the naked octahedral Au_6^{2+} cluster indicated that the non-relativistic description of chemical bonding is unrealistic, because there is significant 6s–5d hybridization in the bonding MOs due to relativistic effects. In a preliminary investigation [31a], the electronic structure of the Au_6^{2+} octahedron was analyzed as a fragment of the C-centered $[Au_6L_6(\mu_6\text{-}C)]^{2+}$ model (with $L=SH_2$ instead of PPh_3 to simplify the calculations). It was found that the relativistic treatment yields the expected increase (by about 0.2) in the 6s Au population, with the 5d Au population decreasing by nearly the same amount. It was pointed out that non-relativistic calculations are adequate for a *qualitative* orbital interaction analysis and offer the advantage of symmetry classification in accordance with a normal point group. Interpretation of the much more complex relativistic orbitals necessitates the use of double groups with their lower number of irreducible representations. Furthermore, substantial spin–orbit interactions in gold atoms introduce additional complications in relativistic calculations. These interactions can be ignored in a qualitative bonding description.

Subsequent calculations [31b] on hypothetical $[Au_6(PH_3)_6(\mu_6\text{-}X)]^n$ analogues (X=B, $n=1+$; X=C, $n=2+$; X=N, $n=3+$) of the known $[Au_6(PPh_3)_6(\mu_6\text{-}C)]^{2+}$ dication were carried out via a self-consistent discrete-variational Xα method with and without relativistic effects. These calculations revealed that the bonding contributions of the 5d Au AOs are as important as those of the 6s Au AOs and that symmetry-dependent 6s–5d gold hybridization leads to tangential Au–Au bonding interactions and a strengthening of the Au–ligand and Au–X bonds. Relativistic effects were found to strongly enhance this interaction mechanism and therefore are significant for the overall stability of gold clusters.

(ii) *The four symmetry-related $Ni_3(CO)_3(\mu_2\text{-}CO)_3$ fragments.* The important frontier SOs for each neutral 42-electron fragment are depicted in Fig. 4; the energies and percent compositions are given in Table 4. The highest filled SO consists of an a_1 combination (under C_{3v} symmetry) of in-plane 3d and 4p Ni AOs. This SO is clearly metal–metal bonding. The lowest unoccupied symmetry orbital (LUSO) of a_2 symmetry is about 4.1 eV higher in energy. It consists of in-plane 3d and 4p Ni AOs and in-plane π^* CO orbitals. This SO is antibonding with respect to Ni–Ni interactions but bonding with respect to Ni–CO interactions. The second lowest unoccupied SO (SLUSO), which lies 0.66 eV above the LUSO, consists of an a_1 combination of the out-of-plane $4p_z$ Ni AOs and out-of-plane π^* CO orbitals. This SO is bonding with respect to both Ni–Ni and Ni–CO interactions. The orbital nature of each of these three frontier orbitals is remarkably analogous to that of the corresponding three frontier orbitals obtained from several extended-Hückel calculations [43] for the $[M_3(CO)_3(\mu_2\text{-}CO)_3]^{0,2-}$ monomers of nickel and platinum; however, the LUMO and SLUMO are reversed in energy, and the HOMO–LUMO gap is much smaller. These energy-level variations of the frontier orbitals may be readily attributed to the extended-Hückel calculations [43] being based upon a planar $M_3(CO)_3(\mu_2\text{-}CO)_3$ moiety of D_{3h} symmetry instead of a non-planar one (with markedly bent (24.1°) bridging

Table 4
Energies and percent compositions of the frontier molecular orbitals for $Ni_3(CO)_6$ under C_{3v} symmetry

MO	Energy (eV)	$3d_{x2-y2}$ (%)	$3d_{xy}$ (%)	$4p_x$,$4p_y$ (%)	$4p_z$ (%)	π^* CO(B) (%)	π^* CO(T) (%)
a_1	−7.93	18.5	18.5	23.6			
a_2	−3.82	9.6	6.4	23.5		39.1	
a_1	−3.16				29.0	29.1	27.9

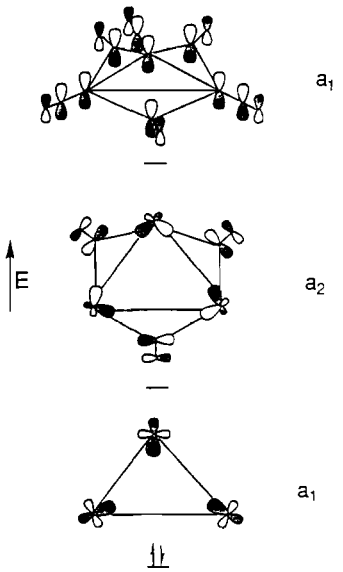

Fig. 4. Frontier molecular orbitals for the neutral $Ni_3(CO)_6$ fragment. Symmetry labels are for an idealized C_{3v} geometry.

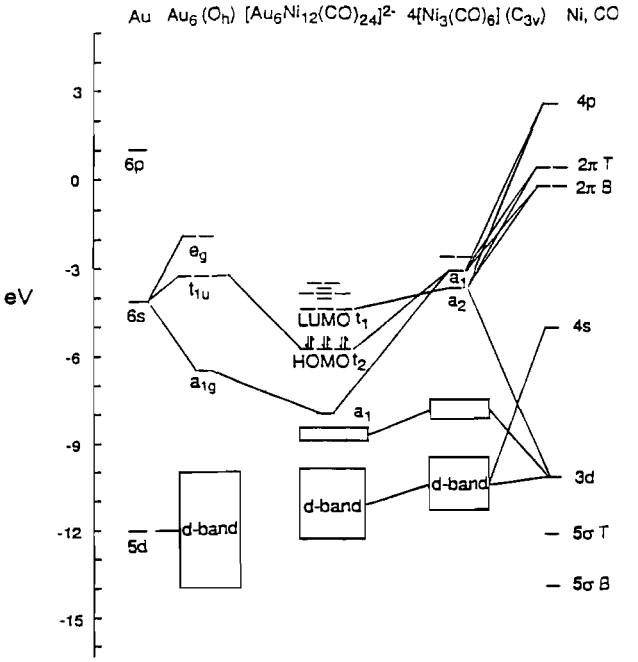

Fig. 5. Molecular orbital correlation diagram for $[Au_6Ni_{12}(CO)_{24}]^{2-}$. The energy levels of the cluster MOs are for the neutral $[Au_6Ni_{12}(CO)_{24}]$ in order to show relative changes in energy arising from orbital interactions of the neutral Au_6 and $Ni_3(CO)_6$ fragments. Two electrons were added to the HOMOs to give the closed-shell configuration of the dianion.

carbonyls) of C_{3v} symmetry in **1** as well as to fundamental differences in the calculation procedures.

3.2.3. The $[Au_6Ni_{12}(CO)_{24}]^{2-}$ cluster

A molecular orbital diagram for the $[Au_6Ni_{12}(CO)_{24}]^{2-}$ dianion is given in Fig. 5. The energies and percent compositions of the important frontier MOs are given in Table 5. This cluster possesses three degenerate HOMOs of t_2 representation, each having approximately 47% gold character (principally antisymmetric combinations of *trans* 6s Au AOs, which are actually non-bonding from orbital overlap considerations, but with some mixing of the higher-lying 6p Au AOs) with the remaining percentage made up of $4p_z$ Ni AOs (25%) and π^* CO orbitals (28%). The SHOMO (second highest occupied molecular orbital) is composed of the totally symmetric bonding combination of the 6s Au AOs (67%) with a mixing of $4p_z$, $3d_{z^2}$ Ni AOs (25%) and π^* CO orbitals (8%); it results from the symmetry-adapted a_1 combination of four identical sets of $Ni_3(CO)_3(\mu_2\text{-}CO)_3$ SOs. Although the SHOMO is primarily a 6s Au–6s Au bonding MO with most of the electron density residing on the Au_6 octahedron, it also contains significant 6s Au–$4p_z$ Ni AO bonding

Table 5
Energies and percent compositions of the frontier molecular orbitals for $[Au_6Ni_{12}(CO)_{24}]^0$ under T_d symmetry

MO	Energy (eV)	Au (%)	Ni (%)	CO (%)
a_1	−8.13	67	25	8
t_2	−5.89	47	25	28
t_1	−4.43	5	49	46

character. An examination of the Au–Ni orbital overlap populations of the SHOMO reveals that the 6s Au–$3d_{z^2}$ Ni AO interactions are essentially zero in contrast to the 6s Au–$4p_z$ Ni AO interactions. These results, which emphasize the relative importance of the more diffuse $4p_z$ Ni AOs in forming stronger Au–Ni bonding interactions at long Au–Ni distances, can be attributed to the relatively high nuclear charges of the

nickel atoms which give rise to highly contracted low-energy 3d Ni AOs.

The cluster possesses three degenerate LUMOs (of t_1 representation) which arise from interactions between the filled in-plane 3d Ni AOs and the (formally) vacant in-plane 4p Ni AOs and π^* CO orbitals, with little contribution from the Au AOs. Thus, the important frontier orbitals in this cluster are composed primarily of 6s Au and 4p Ni AOs with relatively little contribution from the 3d Ni AOs.

The carbonyl ligands play a crucial role in the formation of the Ni–Au bonds. Calculations on the naked Au_6Ni_{12} cluster showed that the 4p Ni AOs are too high in energy to overlap effectively with the gold frontier orbitals, and thereby give rise to Au–Ni bonds. Addition of the π-acidic carbonyl ligands to give four isolated neutral $Ni_3(CO)_3(\mu_2\text{-}CO)_3$ fragments results in favorable interactions of the π^* (CO) orbitals with the 4p Ni AOs, forming four a_1 Ni/CO SOs (under C_{3v} symmetry) which are $\sim$6 eV lower in energy than the isolated degenerate nickel 4p AOs. In turn, these four a_1 SOs of mainly $4p_z$ Ni AOs and out-of-plane π^* (CO) orbitals have the proper symmetry characteristics (a_1 and t_2 under T_d symmetry) and favorable energy-matching to interact with the bonding a_{1g} and non-bonding t_{1u} orbitals of the gold octahedron and to give four frontier MOs (the a_1 SHOMO and t_2 HOMOs) which provide the necessary 'glue' to stabilize this cluster.

It is apparent from the previously described relativistic effects of gold [31, 40a, 41a] that the above non-relativistic bonding description based on the Fenske–Hall model should be appropriately modified via the substitution of 5d–6s hybridized Au orbitals in place of 6s Au AOs. Although the inclusion of 5d–6s hybridized Au orbitals in place of 6s Au AOs would no doubt give rise to considerably stronger Au–Au and Au–Ni bonding interactions, it is our strong prejudice that the overall bonding description and resulting conclusions based upon the Fenske–Hall model are not affected.

3.2.4. *Resulting implications of Fenske–Hall MO calculations*

The necessity of the carbonyl π^* orbitals for the formation of Au–Ni bonding in this cluster may shed light on the curious lack of Au–Ni clusters in the literature. Mixed-metal gold clusters containing late transition metals typically have electron-donating PPh_3 and/or hydride ligands rather than electron-accepting carbonyl ligands. A triphenylphosphine ligand, as a good σ-donor and a relatively weak π-acceptor, would not be expected to stabilize the nickel valence orbitals to the same extent as the carbonyl ligand. The hydride ligand, as a strong σ-donor with no π-accepting ability, would be expected to destabilize the nickel valence orbitals via a build-up of electron density on the nickel atoms. Thus, it becomes apparent that the electronic characteristics of the ligands coordinated to the nickel atoms determine whether or not Au–Ni bonds will be formed.

The unexpected loss of the PPh_3 ligand from the gold atom of the $AuPPh_3Cl$ precursor is also attributed to electronic effects. It was originally thought that reaction of $AuPPh_3Cl$ with the $[Ni_6(CO)_{12}]^{2-}$ dianion would possibly result in the $[PPh_3Au]^+$ moiety bridging triangular faces or edges of a resulting nickel cluster.

The large 1.5 eV HOMO/LUMO gap is consistent with the observed high reduction potential (-1.5 eV versus SCE) indicated from a cyclic voltammogram of the dianion. The triply degenerate LUMOs arise from combination of the $Ni_3(CO)_6$ a_2 orbitals, which are composed of in-plane 3d and 4p Ni AOs and in-plane bridging CO π^* orbitals; these orbitals are bonding with respect to Ni–CO interactions but antibonding with respect to Ni–Ni interactions. The quasi-reversible reduction wave observed in the cyclic voltammogram suggests that population of the triply degenerate LUMOs would probable result in a Jahn–Teller distortion. The irreversible oxidation wave at 1.4 eV suggests that removal of an electron from the triply degenerate HOMOs, which are the principal Au–Ni bonding orbitals, would result in an irreversible alteration in the cluster geometry. The high potential required to oxidize the cluster is consistent with the closed-shell electron count (vide infra), indicating an inherent stability of this cluster.

The shift to higher frequency (by 60 cm^{-1}) of the CO IR absorption bands in the $[Au_6Ni_{12}(CO)_{24}]^{2-}$ dianion relative to those in the $[Ni_6(CO)_{12}]^{2-}$ precursor [10] suggests a substantial withdrawal of electron density from the π^* (CO) orbitals. This may simply be due to the dispersion of the -2 charge over a larger number of metal centers (viz., 12 nickel atoms in $[Au_6Ni_{12}(CO)_{24}]^{2-}$ versus 6 nickel atoms in $[Ni_6(CO)_{12}]^{2-}$ and/or a withdrawal of electron density from the π^* CO orbitals by the electropositive gold core. The Mulliken atomic charge on each gold atom in the cluster was calculated to be $+0.12$, which represents a substantial reduction in positive charge from the formally Au(I) in the $AuPPh_3Cl$ precursor. Indeed, homonuclear gold clusters (e.g., $Au_{11}(PAr_3)_7X_3$ (where Ar = Ph; X = I) [26] and $[Au_9(PPh_3)_8]^{3+}X^-_3$ (where $X = NO_3$) [27]) have been synthesized via reduction of $AuPPh_3X$ with $NaBH_4$, in which the gold atoms have a formal oxidation state between 0 and $+1$. Furthermore, a small quantity of $Au_{11}(PPh_3)_7Cl_3$ was isolated as a minor product (and structurally characterized) from the reaction of $AuPPh_3Cl$ with $[Ni_6(CO)_{12}]^{2-}$. Thus, it would seem probable that the electron-rich $[Ni_6(CO)_{12}]^{2-}$ dianion initially acts as a reducing agent towards $AuPPh_3Cl$, resulting in the formation of the bare gold octahedral core with concomitant conden-

sation of the $Ni_3(CO)_6$ triangles on four faces of the octahedron. Fenske–Hall calculations on the $[Ni_6(CO)_{12}]^{2-}$ dianion (which utilized the same parameters for the $Ni_3(CO)_6$ triangles as were used in the Au_6Ni_{12} cluster) revealed that the negative charge on each nickel atom (−0.16) in the $[Ni_6(CO)_{12}]^{2-}$ dianion is very similar to the negative charge on each nickel atom (−0.18) in the $[Au_6Ni_{12}(CO)_{24}]^{2-}$ dianion; however, the average negative charge on each CO ligand (−0.09) in $[Ni_6(CO)_{12}]^{2-}$ is considerably higher than the average negative charge on each CO ligand (−0.025) in the Au_6Ni_{12} cluster. This charge-density difference indicates a net transfer of electron density from the nickel triangles to the Au_6 core, which is consistent with $[Ni_6(CO)_{12}]^{2-}$ acting as a reducing agent. The reduction in negative charge on the CO ligands upon formation of the $[Au_6Ni_{12}(CO)_{24}]^{2-}$ dianion is also consistent with the upward shift of 60 cm^{-1} in the IR frequencies for the terminal and bridging carbonyl absorption bands relative to those for the $[Ni_6(CO)_{12}]^{2-}$ precursor.

3.3. Application of electron-counting models to the $[Au_6Ni_{12}(CO)_{24}]^{2-}$ dianion

3.3.1. General comments

The observed number of metal cluster valence electrons (CVEs) in this cluster, which may be considered to possess globally delocalized metal–metal bonding, is 236 electrons (i.e., (6×11 (Au)+12×10 (Ni)+24×2 (CO)+2 (charge)=236). We previously pointed out [10] that electron-counting models predict the correct total electron count for *four* vertex-sharing Au_3Ni_3 octahedra but *not* for five face-fused metal octahedra (vide infra). We then concluded that **1** is best considered from an electronic viewpoint as the composite of four vertex-sharing Au_3Ni_3 octahedra. However, the results from the Fenske–Hall model suggest that the stability of **1** arises from delocalized bonding interactions in the frontier MOs involving the central Au_6 octahedron as well as the four Au_3Ni_3 octahedra (which would appear to correspond to the five face-fused octahedral bonding description). In order to resolve this indicated controversy, a bonding analysis of **1** via the different electron-counting schemes (which are outlined elsewhere [44] in applications to a variety of transition metal clusters) is presented herein; based upon this comparison, we propose a qualitative bonding model which (in our view) reconciles electron-counting descriptions of **1** with the MO results.

3.3.2. Polyhedral skeletal electron-pair (PSEP) model

An important extension of this model [45], adopted by Mingos [11] for condensed polyhedra, is the Mingos fusion rule [11c] which treats condensed clusters formally composed of polyhedra that intersect at a vertex, an edge, or a face. According to this rule the sum of the electron counts for the constituent polyhedra minus the electron count for the intersecting set of atoms equals the electron count for the condensed cluster. In the case of four octahedra sharing six vertices, the fusion rule predicts a total of 236 electrons (i.e., (4×86)−(6×18)=236) in agreement with the observed CVE count for **1**. On the other hand, if **1** is depicted as five octahedra sharing four triangular faces, the predicted count is 238 electrons (i.e., (5×86)−(4×48)=238) which is at variance with the observed value. It is noteworthy that this latter total count is based upon the subsequent Mingos proposal [11d, 11g] that the total polyhedral skeletal electron count (c) for a face-condensed polyhedron composed of deltahedra A and B which have six or more vertices can be predicted by use of the general formula $c=a+b-48$ (instead of $c=a+b-50$ [11c]), where a and b are the electron counts of the A and B deltahedra.

3.3.3. Cluster-of-clusters (C^2) model

For this procedure developed by Teo and Zhang [12], **1** is considered as a *supracluster* formed by n polyhedral clusters. In general, the total number of electron pairs (T) is given by $T=6V_m+V_n+B$, where V_m and V_n are the number of transition metal and main-group vertices, respectively, in the cluster. The value B is the number of (filled) bonding cluster valence orbitals formed by the $3V$ cluster orbitals (where $V=V_m+V_n$), which in the context of the PSEP model corresponds to the number of apparent skeletal electron pairs. In the case of a supracluster (s_n), defined as a cluster of n smaller cluster units fused together via vertex-, edge-, or face-sharing, B may be obtained as the sum of the skeletal electron pairs (B_j) of the individual cluster units minus the overcounted skeletal electron pairs (B_k) of the shared vertices, edges, or faces (corresponding to three, five, and six electron pairs, respectively).

For four Au_3Ni_3 octahedra in **1** sharing six (gold) vertices, the total number of skeletal electron pairs is given by $B=4\times7$ (oct.)-6×3 (shared vertices)$=10$. Here each octahedron contributes 7 skeletal electron pairs, and each of the six shared vertices overcounts by 3 electron pairs. Since $V_m=18$ and $V_n=0$, the total number of electron pairs is given by $T=6V_m+B=(6\times18)+10=118$, which results in the correct total electron count of $N=2T=236$. The alternative description of *five* metal octahedra sharing four triangular faces gives a predicted electron count (N) of 238 (viz., $B=5\times7$ (oct.)-4×6 (shared faces)$=11$; $T=6V_m+B=(6\times18)+11=119$; and $N=2T=238$) which is two electrons in excess of the observed value.

3.3.4. Graph-theory derived model

In this model developed by King [13], the valence orbitals of the atoms in the metal clusters are partitioned into internal and external orbitals. Internal orbitals participate in the metal cluster skeletal bonding, while external orbitals participate in metal–ligand bonding. In the case of a globally delocalized transition metal carbonyl cluster consisting of fused octahedra, King [13i] makes the following assumptions: (i) each vertex unique to a single octahedron uses three internal orbitals; (ii) the common vertex between two vertex-sharing octahedra (11 vertices) uses *six* internal orbitals, viz. three for the skeletal bonding in each octahedron; (iii) each of the two common vertices between two edge-sharing octahedra (10 vertices) uses *five* internal orbitals, viz. one for the six-center, two-electron core bonding orbital (a_{1g}) in each octahedron, two for surfacc bonding, and one for forming the two-center, two-electron bond along the shared edge; (iv) each of the three common vertices between two face-sharing octahedra uses *four* internal orbitals, viz. one for the six-center, two-electron core bonding in each octahedron and two for surface bonding. Particularly noteworthy is that in the cases where the number of internal orbitals per vertex determined by the King model differs from the *normal three per vertex*, it follows that the resulting number of skeletal electron paris obtained from the King model does *not* correspond to the apparent number obtained from both the PSEP and cluster-of-cluster models (i.e., these latter models generally assume that each transition metal vertex uses only *three* internal orbitals and has the usual 18-electron noble-gas electronic configuration).

Of special importance to our reinterpretation of the PSEP and cluster-of-clusters electron-counting models for $[Au_6Ni_{12}(CO)_{24}]^{2-}$ (vide infra) is the recent modification and extension by King [13i] of his graph-theoretical treatment of fused octahedral metal clusters to account for thc obscrvation that both the face-fused bioctahedral Ir_9 core in $[Ir_9(CO)_{20}]^{3-}$ [46] and the face-fused trioctahedral Ir_{12} core in $[Ir_{12}(CO)_{26}]^{2-}$ [47] have two more apparent skeletal electrons than the corresponding structurally analogous Rh_9 and Rh_{12} cores in $[Rh_9(CO)_{19}]^{3-}$ [48] and $H_2Rh_{12}(CO)_{25}$ [49], respectively. This difference in apparent skeletal electron counts between these analogous rhodium and iridium clusters was attributed by King [13i] to the presence of much stronger interactions between the six-center core bonding orbitals in adjacent octahedra in the rhodium clusters relative to those in the corresponding iridium clusters. Thus, King [13i] proposed that for both $[Ir_9(CO)_{20}]^{3-}$ and $[Ir_{12}(CO)_{26}]^{2-}$ there are *insignificant* interoctahedral interactions between the fully symmetric six-center S^{σ} core orbitals in adjacent octahedra; consequently, the combinations of these S^{σ} core orbitals remain essentially non-bonding, and each combination thereby accommodates an electron pair. However, strong interoctahedral interactions were postulated for the two face-fused Rh_9 octahedra in $[Rh_9(CO)_{19}]^{3-}$ such that the antibonding combination of the two S^{σ} orbitals no longer possesses an electron pair. Likewise, it was proposed for the three face-fused Rh_{12} octahedra in $H_2Rh_{12}(CO)_{25}$ that strong interactions among the three core S^{σ} orbitals in the three octahedral cavities result in only the formally bonding and non-bonding combinations (but not the antibonding combination) being occupied by electron pairs. Hence, this King model [13i] suggests that both $[Rh_9(CO)_{19}]^{3-}$ and $H_2Rh_{12}(CO)_{25}$ can be regarded as missing one pair of core-bonding electrons.

In the specific application of his model to the $[Au_6Ni_{12}(CO)_{24}]^{2-}$ dianion, King [13i] utilized the following sources of internal orbitals and valence electrons: (i) each of 12 $Ni(CO)_2$ vertices belonging to one of the four Au_3Ni_3 octahedra uses three orbitals and provides two electrons; (ii) each of six Au vertices shared between two Au_3Ni_3 octahedra uses six orbitals and provides five electrons; (iii) the -2 anionic charge provides two electrons. This electron-counting scheme gives rise to a composite total of 72 internal orbitals (i.e., $12(3)+6(6)=72$) and 56 valence electrons (i.e., $12(2)+6(5)+2=56$). The 72 internal orbitals and 56 electrons were used in each of the four Au_3Ni_3 octahedra to form one six-center, two-electron bond (24 orbitals; 8 electrons) and six two-electron surface bonds (48 orbitals; 48 electrons). Because the internal orbitals and skeletal electrons required for the globally delocalized bonding in this cluster matched exactly to those available, King [13i] concluded that this cluster is orbital- and electron-precise. King [13i] stated that his bonding scheme was based upon two assumptions: (i) six of the eleven valence electrons of each bare gold atom with six internal orbitals are required for its $9-6=3$ external orbitals, leaving $11-6=5$ skeletal electrons available from each gold vertex; (ii) each of the four Au_3Ni_3 octahedra contains a six-center, two-electron bond, but the central Au_6 octahedron does *not* contain a multicenter core bond. He further pointed out that the distance between the core molecular S^{σ} orbitals (vide infra) in the four tetrahedrally oriented Au_3Ni_3 octahedra is "much too far for any interaction between them". His second assumption and the above-mentioned conclusion are of particular relevance to our reinterpretation of the PSEP and cluster-of-cluster models in terms of a model involving five face-fused octahedra which is shown to be in accordance with the results of the Fenske–Hall MO calculations.

3.4. Proposed reconcilability of the face-fused octahedral bonding description of $[Au_6Ni_{12}(CO)_{24}]^{2-}$ via electron-counting models with the Fenske–Hall MO results

Since none of the electron-counting procedures predicts the observed valence electron total for five face-

fused metal octahedra, we suggested in our preliminary report [10] that this Au–Ni dianion is best considered from a bonding viewpoint as the composite of four vertex-sharing Au_3Ni_3 octahedra. However, the orbital character obtained via the Fenske–Hall MO calculations for the filled a_1 SHOMO, shown in the MO correlation diagram (Fig. 5), is %Au = 67, %Ni = 25, %CO = 8. Similarly, for the t_2 HOMOs, the orbital character is %Au = 46, %Ni = 25, %CO = 28. On this basis we conclude that the totally symmetric (a_1) multicenter, two-electron bonding SHOMO includes the central Au_6 octahedron as well as the four Au_3Ni_3 octahedra. In this connection, it is especially noteworthy that King [13i] rationalized that the missing pair of core bonding electrons in both $[Rh_9(CO)_{19}]^{3-}$ and $H_2Rh_{12}(CO)_{25}$ is a consequence of relatively strong interactions between the S^σ core MOs in adjacent face-fused octahedra which raise the energy of one of these MOs to an antibonding (and hence unoccupied) level. One can likewise rationalize that a similar phenomenon occurs in the Au_6Ni_{12} cluster such that the symmetrical Au_6 octahedral a_1 combination combines with the symmetrical a_1 combination of the four Au_3Ni_3 octahedra to give an occupied bonding MO and an empty antibonding MO. Hence, the a_1 SHOMO and t_2 HOMOs for the Au_6Ni_{12} dianion correspond in each electron-counting scheme to the four multicenter, two-electron core bonds. These four frontier MOs, which mainly involve bonding 6s Au–6s Au and 6s Au–4p_z Ni AO bonding interactions in the interoctahedral core-binding a_1 combination (viz., the SHOMO) and 6s Au–4p_z Ni AO bonding interactions in the core-bonding t_2 combinations (viz., the three degenerate HOMOs), are the major contributors in accounting for the existence of this Au–Ni cluster. It is noteworthy that the inclusion of relativistic effects would give rise to a considerably greater binding energy via strongly enhanced 6s–5d gold hybridization, which in turn would strengthen both the Au–Au and Au–Ni bonding interactions.

This interoctahedral bonding model involving four S^σ core-bonding electron pairs for the five face-fused octahedra in **1** is also consistent with the similar bonding descriptions proposed from different theoretical treatments [43a, 50–53] for the triangular-metal stacking geometries of the $[M_3(CO)_3(\mu_2\text{-}CO)_3]_n^{2-}$ oligomers (M = Ni, Pt; n = 2,3). In the case of the trigonal-antiprismatic $[Ni_6(CO)_{12}]^{2-}$ dianion, extended-Hückel calculations [43a, 50], pseudo-potential calculations [51], local density functional (LCGTO/LDF) calculations [52], and Fenske–Hall calculations [53] all indicated that the major contributor to the binding energy or 'glue' holding the two $Ni_3(CO)_3(\mu_2\text{-}CO)_3$ interlayers together is the totally symmetrical HOMO containing the extra electron pair (due to the −2 charge); furthermore, this in-phase bonding combination, composed predominantly of out-of-plane 4p_z Ni AOs and π^* μ_2-CO orbitals, may likewise be considered as an octahedral-like S^σ core-bonding MO.

The fact that the interoctahedral bonding model applied to the five face-fused metal octahedra in $[Au_6Ni_{12}(CO)_{24}]^{2-}$ gives rise to a total electron count of 236 valence electrons in agreement with the observed electron count is important from two viewpoints. It not only reconciles the PSEP and cluster-of-clusters electron-counting methods with the Fenske–Hall MO results but also indicates that (contrary to our earlier suggestion [10]) one cannot necessarily conclude from electronic considerations that **1** is best considered as the composite of four vertex-sharing Au_3Ni_3 octahedra. Hence, this comparative analysis emphasizes that electron-counting procedures do not necessarily provide an unambiguous physical picture concerning the nature of the electron-pair distributions in a transition metal cluster. This conclusion is consistent with the view expressed by Woolley [54] that the isolobal principle and electron-counting rules owe their generality and utility to being symmetry-based, but that the energetics and details of the electronic structures of transition metal clusters are a separate matter requiring appropriate methods of theoretical chemistry.

3.5. Physical properties of the $[Au_6Ni_{12}(CO)_{24}]^{2-}$ dianion and resulting surface-science implications of its bimetallic core

The Au_6Ni_{12} core may be considered as a segregated bimetallic phase, in which the central Au_6 core is encased in a layer of twelve nickel atoms, such that the gold and nickel may be considered to be immiscible components. Other mixed-metal carbonyl clusters with segregated bimetallic cores include the $[Pd_6Fe_6(CO)_{24}H]^{3-}$ trianion with a trigonal-antiprismatic (octahedral) Pd_6 kernel [55], the $[Pt_6Ni_{38}(CO)_{52}H_x]^{4-x}$ anions with an octahedral Pt_6 kernel [56] and the $[Rh_5Ni_6(CO)_{21}H_x]^{3-}$ trianion with a trigonal-bipyramidal Rh_5 kernel [57]. In the case of **1**, the octahedral gold kernel of each Au_6Ni_{12} particle of pseudo-cubic T_d symmetry is encapsulated by 12 symmetry-equivalent Ni surface atoms. The geometrical arrangement of the nickel atoms can be described in terms of a T_d-distorted polyhedron of the 3^24^2 cuboctahedron, a semi-regular centrosymmetric polyhedron of cubic O_h symmetry with 12 vertices, 6 square and 8 equilateral triangular faces, and 24 edges [58]. The particular cubic T_d distortion giving rise to the 12-vertex nickel polyhedron in **1** involves the compression of 12 edges comprising one set of alternate triangular faces and concomitant expansion of the 12 edges comprising the other set of alternate triangular faces. The particle size of this non-centrosymmetric Au_6-centered nickel polyhedron varies from 5.8 Å in diameter between the two centroids of the opposite compressed and elongated triangular faces along each

of the four body-diagonal C_3-3 ⟨111⟩ axes to 5.0 Å in diameter between the two centroids of the rectangular faces along each of the three S_4-$\bar{4}$ ⟨100⟩ axes.

1 may be considered to be a molecular analog to the 'chemisorption-induced aggregation' (CIA) model experimentally documented from surface-science studies [59] for other bimetallic systems containing Group VIII (8–10) metal–Group IB (11) metal atoms. The normal surface-enrichment composition rule invoked for bimetallic particles (under ultrahigh vacuum) states that the metal component with the lower heat of sublimation (i.e., normally weaker metal–metal interactions) should concentrate at the surface in order to lower the surface tension. However, according to the thermodynamic-based CIA model [60], the surface-enrichment composition can be reversed if an absorbate gas binds much more strongly to the other metal component with the higher heat of sublimation [61]. Thus, for Ni–Au alloys (and in general for other Group VIII (8–10) metal–Group IB (11) metal alloys) under an inert atmosphere, the surface-science rule predicts that the gold atoms would concentrate at the surface because the Group 11 gold has a lower sublimation energy than the Group 10 nickel. However, Auger electron spectroscopic studies of Ni–Au alloys [59c] have given evidence for dramatic changes in surface composition upon oxygen chemisorption. Since the nickel–oxygen bond is stronger than the gold–oxygen bond [62], the surface becomes expectedly nickel-rich. Hydrogen chemisorption also causes nickel enrichment at the surface, but to a lesser extent than for oxygen chemisorption; this variation was attributed to the nickel–hydrogen bond being stronger than the gold–hydrogen bond but the difference in bond strengths being less than that for the case of oxygen chemisorption. The fact that carbon monoxide chemisorbs strongly and selectively to platinum (a congener of nickel) rather than to gold results in the expectation that a CO atmosphere would lead to an enrichment of platinum atoms at the surface. This phenomenon was observed for Pt–Au alloys in ultrahigh vacuum and in the presence of CO [59a].

It is presumed in **1** that the nickel-coordinated carbonyl ligands play an analogous role. A similar reversal of surface composition has been observed for the $[Ag_{13}Fe_8(CO)_{32}]^{4-}$ tetraanion [63], which contains an Ag_{13} centered cuboctahedron with each triangular face capped by an $Fe(CO)_4$ group, and for the $[Cu_6Fe_4(CO)_{16}]^{2-}$ dianion [64], which contains a Cu_6 octahedron capped on each of four alternating faces by an $Fe(CO)_4$ fragment.

Attempts to synthesize silver and copper analogues of $[Au_6Ni_{12}(CO)_{24}]^{2-}$ by reactions of $[PPh_3AgI]_4$ and $(PPh_3)_3CuCl$ with $[Ni_6(CO)_{12}]^{2-}$ were unsuccessful. No reaction was observed at room temperature in THF with the copper reagent, while reactions with the silver reagent produced $[Ni_9(CO)_{18}]^{2-}$, which has been obtained previously [36] via oxidation of $[Ni_6(CO)_{12}]^{2-}$. Preliminary Fenske–Hall calculations on the hypothetical $[Ag_6Ni_{12}(CO)_{24}]$ cluster indicated that formation of an Ag_6 octahedron is not favored because the highest occupied t_{1u} SOs, which are non-bonding in the Au_6 octahedron, are strongly antibonding in the Ag_6 octahedron.

Acknowledgements

We greatly appreciate the financial support of this research by the National Science Foundation (Grants CHE-9013059, 9310428). Purchase of the X-ray diffractometry equipment and associated computers was made possible by funds from NSF (Grant CHE-9105497) and from the Graduate School (UW-Madison). One of us (A.J.W.) is grateful to the Graduate School (UW-Madison) for a first-year Graduate Fellowship (Sept. 1989–Aug. 1990) and to the Department of Education for a DOE Fellowship (Sept. 1991–Aug. 1992; Jan. 1993–May 1993). We are also indebted to Dr Randy K. Hayashi for assistance in the X-ray crystallographic aspects of this work, to Dr Jeffrey P. Zebrowski for helpful synthetic advice, to Professor Boon K. Teo (University of Illinois at Chicago) for informative discussions on the application of the Teo–Zhang cluster-of-clusters electron-counting model to the $[Au_6Ni_{12}(CO)_{24}]^{2-}$ dianion, and to Professor R. Bruce King (University of Gerogia) for a preprint (Ref. [13i]) of his paper on 'Metal Cluster Topology. 14. Fusion of octahedra in metal carbonyl clusters'. We are also most pleased to acknowledge AESAR/Johnson Matthey (Ward Hill, MA) for their University Metal Loans Program in providing a sample of auric acid, from which Ph_3PAuCl was prepared.

References

[1] A.M. Mueting, W. Bos, B.D. Alexander, P.D. Boyle, J.A. Casalnuovo, S. Balaban, L.N. Ito, S.M. Johnson and L.H. Pignolet, *New J. Chem., 12* (1988) 505, and refs. therein.

[2] (a) J.H. Sinfelt, *Bimetallic Catalysts,* Wiley, New York, 1983, Chs. 1 and 2; (b) I.E. Wachs, *Gold Bull., 16* (1983) 98.

[3] (a) J. Evans and G. Jingxing, *J. Chem. Soc., Chem. Commun.,* (1985) 39; (b) Exxon Research and Engineering Co., *Eur. Patent No. 37 700; US Patent No. 4 301 086, US Patent No. 4 342 838;* (c) Union Carbide Corp., *US Patent No. 3 878 292;* (d) P.D. Alexander, M.P. Gomez-Sal, P.R. Gannon, C.A. Blaine, P.D. Boyle, A.M. Mueting and L.H. Pignolet, *Inorg. Chem., 27* (1988) 3301.

[4] P. Braunstein and J. Rose, in I. Bernal (ed.), *Stereochemistry of Organometallic and Inorganic Compounds,* Vol. 3, Elsevier, Amsterdam, 1988.

[5] J. Schwank, *Gold Bull., 18* (1985) 1.

[6] (a) L.N. Ito, J.D. Sweet, A.M. Mueting, L.H. Pignolet, M.F. Schoondergang and J.J. Steggerda, *Inorg. Chem., 28* (1989) 3696; (b) L.N. Ito, B.J. Johnson, A.M. Mueting and L.H.

Pignolet, *Inorg. Chem., 28* (1989) 2026; (c) P.D. Boyle, D.C. Boyd, A.M. Mueting and L.H. Pignolet, *Inorg. Chem., 27* (1988) 4424; (d) P.D. Boyle, B.J. Johnson, B.D. Alexander, J.A. Casalnuovo, P.R. Gannon, S.M. Johnson, E.A. Larka, A.M. Mueting and L.H. Pignolet, *Inorg. Chem., 26* (1987) 1346; (e) B.D. Alexander, P.D. Boyle, B.J. Johnson, S.M. Johnson, J.A. Casalnuovo, A.M. Mueting and L.H. Pignolet, *Inorg. Chem., 26* (1987) 2547; (f) B.D. Alexander, B.J. Johnson, S.M. Johnson, A.L. Casalnuovo and L.H. Pignolet, *J. Am. Chem. Soc., 109* (1986) 4409; (g) P.D. Boyle, B.J. Johnson, A. Buehler and L.H. Pignolet, *Inorg. Chem., 25* (1986) 5; (h) A.L. Casalnuovo, J.A. Casalnuovo, P.V. Nilsson and L.H. Pignolet, *Inorg. Chem., 24* (1985) 2554; (i) M.A. Aubart and L.H. Pignolet, *J. Am. Chem. Soc., 114* (1992) 7901; (j) T.G.M.M. Kappen, J.J. Bour, P.P.J. Schlebos, A.M. Roelofsen, J.G.M. van der Linden, J.J. Steggerda, M.A. Aubart, D.A. Krogstad, M.F.J. Schoondergang and L.H. Pignolet, *Inorg. Chem., 32* (1993) 1074.

[7] (a) B.K. Teo and K. Keating, *J. Am. Chem. Soc., 106* (1984) 2224; (b) B.K. Teo, M. Hong, H. Zhang, D. Huang and X. Shi, *J. Chem. Soc. Chem. Commun.,* (1988) 204; (c) B.K. Teo, H. Zhang and X. Shi, *Inorg. Chem., 29* (1990) 2083; (d) B.K. Teo, M. Hong, H. Zhang and D. Huang, *Angew. Chem., Int. Ed. Engl., 26* (1987) 897; (e) B.K. Teo, *Polyhedron, 7* (1988) 2317; (f) B.K. Teo, H. Zhang and X. Shi, *J. Am. Chem. Soc., 112* (1990) 8552; (g) B.K. Teo, X. Shi and H. Zhang, *J. Am. Chem. Soc., 113* (1991) 4329; (h) B.K. Teo and H. Zhang, *Proc. Natl. Acad. Sci. USA, 88* (1991) 5067; (i) B.K. Teo, X. Shi and H. Zhang, *Inorg. Chem., 32* (1993) 3987; (j) B.K. Teo, H. Zhang and X. Shi, *J. Am. Chem. Soc., 115* (1993) 8489; (k) T.G.M.M. Kappen, P.P.J. Schlebos, J.J. Bour, W.P. Bosman, J.M.M. Smits, P.T. Beurskens and J.J. Steggerda, *Inorg. Chem., 33* (1994) 754.

[8] K.P. Hall and D.M.P. Mingos, *Prog. Inorg. Chem., 32* (1984) 237, and refs. therein.

[9] M.B. Hall and R.F. Fenske, *Inorg. Chem., 11* (1972) 768.

[10] A.J. Whoolery and L.F. Dahl, *J. Am. Chem. Soc., 113* (1991) 6683.

[11] (a) D.G. Evans and D.M.P. Mingos, *J. Organomet. Chem., 240* (1982) 321; (b) *Organometallics, 2* (1983) 235; (c) D.M.P. Mingos, *J. Chem. Soc., Chem. Commun.,* (1983) 706; (d) *Acc. Chem. Res., 17* (1984) 311; (e) D.M.P. Mingos, *Inorg. Chem., 24* (1985) 114; (f) R.L. Johnston and D.M.P. Mingos, *J. Organomet. Chem., 280* (1985) 407; (g) *J. Organomet. Chem., 280* (1985) 419; (h) D.M.P. Mingos, *J. Chem. Soc., Chem. Commun.,* (1985) 1352; (i) R.L. Johnston and D.M.P. Mingos, *J. Chem. Soc., Dalton Trans.,* (1987) 1445; (j) D.M.P. Mingos and L. Zenyang, *J. Chem. Soc., Dalton Trans.,* (1988) 1657; (k) D.M.P. Mingos and A.P. May, in D.F. Shriver, H.D. Kaesz and R.D. Adams (eds.), *The Chemistry of Metal Cluster Complexes,* VCH, New York, 1990, Ch. 2, pp. 11–119; (l) D.M.P. Mingos and D.J. Wales, *Introduction to Cluster Chemistry,* Prentice Hall, Old Tappan, NJ, 1990.

[12] (a) B.K. Teo and H. Zhang, *Polyhedron, 9* (1990) 1985; (b) *Inorg. Chim. Acta, 144* (1988) 173; (c) *Inorg. Chem., 27* (1988) 414.

[13] (a) R.B. King and D.H. Rouvray, *J. Am. Chem. Soc., 99* (1977) 7834; (b) R.B. King, in R.B. King (ed.), *Chemical Applications of Topology and Graph Theory,* Elsevier, Amsterdam, 1983, pp. 99–123; (c) in J.F. Liebman and A. Greenberg (eds.), *Molecular Structure and Energetics,* Vol. 1, VCH, Deerfield Beach, FL, pp. 123–148; (d) in P. Jena, B.K. Rao and S.N. Khanna (eds.), *The Physics and Chemistry of Small Clusters,* Plenum, New York, 1987, pp. 79–82; (e) *J. Phys. Chem., 92* (1988) 4452; (f) *Isr. J. Chem., 30* (1990) 315; (g) *J. Chem. Inf. Comput. Sci., 32* (1992) 42; (h) *Acc. Chem. Res., 25* (1992) 247; (i) *Inorg. Chim. Acta, 212* (1993) 57.

[14] (a) J.C. Calabrese, L.F. Dahl, A. Cavalieri, P. Chini, G. Longoni and S. Martinengo, *J. Am. Chem. Soc., 96* (1974) 2616; (b) G. Longoni, P. Chini and A. Cavalieri, *Inorg. Chem., 15* (1976) 3025.

[15] A.G. Jones and D.G. Powell, *Spectrochim. Acta, Part A, 30* (1974) 563.

[16] R.L. Bedard and L.F. Dahl, *J. Am. Chem. Soc., 108* (1986) 5933.

[17] P. He, J.P. Avery and L.R. Faulkner, *Anal. Chem., 54* (1982) 1313A.

[18] *SHELXTL-PLUS*, Siemens Analytical X-ray Instruments, Inc., Madison, WI, USA.

[19] A.J. Whoolery, *Ph.D. Dissertation,* University of Wisconsin-Madison, WI, USA, 1993.

[20] (a) A.L. Sargent and M.B. Hall, *Polyhedron, 9* (1990) 1799; (b) Z. Lin and M.B. Hall, *Inorg. Chem., 30* (1991) 3817.

[21] (a) R.F. Fenske, *Prog. Inorg. Chem., 21* (1976) 179; (b) *Pure Appl. Chem., 27* (1971) 61; (c) *60* (1988) 1153.

[22] B.E. Bursten, *Pure Appl. Chem., 63* (1991) 839.

[23] (a) J.L. Petersen, D.L. Lichtenberger, R.F. Fenske and L.F. Dahl, *J. Am. Chem. Soc., 97* (1975) 6433; (b) H.A. Harris, D.R. Kanis and L.F. Dahl, *J. Am. Chem. Soc., 113* (1991) 8602; (c) T.E. North, J.B. Thoden, B. Spencer and L.F. Dahl, *Organometallics, 12* (1993) 1299.

[24] F. Herman and S. Skillman, *Atomic Structure Calculations,* Prentice Hall, Englewood Cliffs, NJ, 1963.

[25] (a) B.E. Bursten and R.F. Fenske, *J. Chem. Phys., 67* (1977) 3138; (b) B.E. Bursten, J.R. Jensen and R.F. Fenske, *J. Chem. Phys., 68* (1978) 3320.

[26] (a) V.G. Albano, P.L. Bellon, M. Manassero and M. Sansoni, *J. Chem. Soc., Chem. Commun.,* (1970) 1210; (b) F. Cariati and L. Naldini, *Inorg. Chim. Acta, 5* (1971) 172.

[27] (a) P.L. Bellon, F. Cariati, M. Manassero, L. Naldini and M. Sansoni, *J. Chem. Soc., Chem. Commun.,* (1971) 1423; (b) F. Cariati and L. Naldini, *J. Chem. Soc., Dalton Trans.,* (1972) 2286.

[28] (a) P.L. Bellon, M. Manassero, L. Naldini and M. Sansoni, *J. Chem. Soc., Chem. Commun.,* (1972) 1035; (b) P. Bellon, M. Manassero and M. Sansoni, *J. Chem. Soc., Dalton Trans.,* (1973) 2423.

[29] F. Scherbaum, A. Grohmann, B. Huber, C. Krüger and H. Schmidbaur, *Angew. Chem., Int. Ed. Engl., 27* (1988) 1544.

[30] (a) D.M.P. Mingos, *J. Chem. Soc., Dalton Trans.,* (1976) 1163; (b) *Nature (London), 345* (1990) 113.

[31] (a) N. Rösch, A.Görling, D.E. Ellis and H. Schmidbaur, *Angew. Chem., Int. Ed. Engl., 28* (1989) 1357; (b) A. Görling, N. Rösch, D.E. Ellis and H. Schmidbaur, *Inorg. Chem., 30* (1991) 3986.

[32] D.M.P. Mingos and R.P.F. Kanters, *J. Organomet. Chem., 384* (1990) 405.

[33] (a) H. Schmidbaur, *Gold Bull., 23* (1990) 11; (b) H. Schmidbaur, B. Brachthäuser and O. Steigelmann, *Angew. Chem., Int. Ed. Engl., 30* (1991) 1488; (c) H. Schmidbaur, B. Brachthäuser, O. Steigelmann and H. Beruda, *Chem. Ber., 125* (1992) 2705; (d) O. Steigelmann, P. Bissinger and H. Schmidbaur, *Angew. Chem., Int. Ed. Engl., 29* (1990) 1399; (f) A. Grohmann, J. Riede and H. Schmidbaur, *Nature (London), 345* (1990) 140; (g) F. Scherbaum, A. Grohmann, G. Müller and H. Schmidbaur, *Angew. Chem., Int. Ed. Engl., 28* (1989) 463; (h) H. Schmidbaur, W. Graf and G. Müller, *Angew. Chem., Int. Ed. Engl., 27* (1988) 417; (i) H. Schmidbaur, F. Scherbaum, B. Huber and G. Müller, *Angew. Chem., Int. Ed. Engl., 27* (1988) 419; (i) H. Schmidbaur, C. Hartmann, G. Reber and G. Müller, *Angew. Chem., Int. Ed. Engl., 26* (1987) 1146; (j) M. Nakamoto, W. Hiller and H. Schmidbaur, *Chem. Ber., 126* (1993) 605.

[34] (a) M. Ahlgren, T.T. Pakkanen and A. Tahranainet, *J. Organomet. Chem., 323* (1987) 91; (b) M.I. Bruce and B.K. Nicholson, *Organometallics, 3* (1984) 101; (c) P. Braunstein, J.

Rose, A. Dedieu, J. Dusausoy, A. Mangeot and M. Tiripicchio-Camellini, *J. Chem. Soc., Dalton Trans.,* (1986) 225; (d) J.W.A. van der Velden, J.J. Bour, B.F. Otterloo, W.P. Bosman and J.H. Noordik, *J. Chem. Soc., Chem. Commun.,* (1981) 583; (e) E. Roland, K. Fischer and H. Vahrenkamp, *Angew. Chem., Int. Ed. Engl., 22* (1983) 326; (f) J.W. Lauher and K. Wald, *J. Am. Chem. Soc., 103* (1981) 7648.

[35] O.M. Abu-Salah, A.-R.A. Al-Ohaly and C.B. Knobler, *J. Chem. Soc., Chem. Commun.,* (1985) 1502.

[36] (a) D.A. Nagaki, L.D. Lower, G. Longoni, P. Chini and L.F. Dahl, *Organometallics, 5* (1986) 1764; (b) G. Longoni and P. Chini, *Inorg. Chem., 15* (1976) 3029.

[37] (a) R.W. Broach, L.F. Dahl, G. Longoni, P. Chini, A.J. Schultz and J.M. Williams, *Adv. Chem. Ser., No. 167* (1978) 93; (b) P. Chini, G. Longoni, M. Manassero and M. Sansoni, *Abstr., Eighth Meet. Italian Association of Crystallography, Ferrara, Italy, 1977,* Communication No. 34; (c) A. Ceriotti, P. Chini, R.D. Pergola and G. Longoni, *Inorg. Chem., 22* (1983) 1595; (d) D.A. Nagaki and L.F. Dahl, unpublished research, 1986.

[38] (a) P. Pyykkö, *Chem. Rev., 88* (1988) 563; (b) V. Bonacic-Koutecky, P. Fantucci and J. Koutecky, *Chem. Rev., 91* (1991) 1035; (c) K.S. Pitzer, *Acc. Chem. Res., 12* (1979) 271.

[39] (a) K. Balasubramanian, *J. Phys. Chem., 93* (1989) 6585; (b) K. Balasubramanian, *J. Mol. Struct. (Theochem.), 202* (1989) 291.

[40] (a) P. Schwerdtfeger, M. Dolg, W.H.E. Schwarz, G.A. Bowmaker and P.D.W. Boyd, *J. Chem. Phys., 91* (1989) 1762; (b) P. Schwerdtfeger, *J. Am. Chem. Soc., 111* (1989) 7261; (c) P. Schwerdtfeger, P.D.W. Boyd, A.K. Burrell, W.T. Robinson and M.J. Taylor, *Inorg. Chem., 29* (1990) 3593; (d) P. Schwerdtfeger and P.D.W. Boyd, *Inorg. Chem., 31* (1992) 327.

[41] (a) P. Pyykkö and Y. Zhao, *Angew. Chem., Int. Ed. Engl., 30* (1991) 604; (b) *Chem. Phys. Lett., 177* (1991) 103.

[42] (a) D.-W. Liao and K. Balasubramanian, *J. Chem. Phys., 97* (1992) 2548; (b) K. Balasubramanian and D.-W. Liao, *J. Chem. Phys., 94* (1991) 5233; (c) R. Arratia-Perez and G.L. Malli, *Chem. Phys. Lett., 125* (1986) 143; (d) G.F. Gantefor, D.M. Cox and A. Kaldor, *J. Chem. Phys., 96* (1992) 4102; (e) K.J. Taylor, C. Jin, J. Conceicao, L.-S. Wang, O. Cheshnovsky, B.R. Johnson, P.J. Nordlander and R.E. Smalley, *J. Chem. Phys., 93* (1990) 7515.

[43] (a) D.J. Underwood, R. Hoffmann, K. Tatsumi, A. Nakamura and Y. Yamamoto, *J. Am. Chem. Soc., 107* (1985) 5968; (b) C. Mealli, *J. Am. Chem. Soc., 107* (1985) 2245; (c) J. Evans, *J. Chem. Soc., Dalton Trans.,* (1980) 1005.

[44] K.C.C. Kharas and L.F. Dahl, *Adv. Chem. Phys., 70* (Part 2) (1988) 1.

[45] (a) K. Wade, *J. Chem. Soc., Chem. Commun.,* (1971) 792; (b) *Electron Deficient Compounds,* Thomas Nelson, London, 1971; (c) *Chem. Br., 11* (1975) 177; (d) *Adv. Inorg. Chem. Radiochem., 18* (1976) 1; (e) D.M.P. Mingos, *Nature (London), Phys. Sci., 236* (1972) 99; (f) D.M.P. Mingos and M.I. Forsyth, *J. Chem. Soc., Dalton Trans.,* (1977) 610; (g) M.E. O'Neill and K. Wade, *Inorg. Chem., 21* (1982) 464; (h) M. E. O'Neill and K. Wade, *Polyhedron, 2* (1983) 963.

[46] R. Della Pergola, F. Demartin, L. Garlaschelli, M. Manassero, S. Martinengo, N. Masciocchi and D. Strumolo, *Inorg. Chem., 30* (1991) 846.

[47] R. Della Pergola, F. Demartin, L. Garlaschelli, M. Manassero, S. Martinengo and M. Sansoni, *Inorg. Chem., 26* (1987) 3487.

[48] S. Martinengo, A. Fumagalli, R. Bonfichi, G. Ciani and A. Sironi, *J. Chem. Soc., Chem. Commun.,* (1982) 825.

[49] G. Ciani, A. Seroni and S. Martinengo, *J. Chem. Soc., Chem. Commun.,* (1985) 1757.

[50] N.A. McEvoy, D.G. Evans and D.M.P. Mingos, unpublished results (cited in Ref. [15] of paper by Hoffmann and co-workers [43a]).

[51] D.W. Bullett, *Chem. Phys. Lett., 115* (1985) 450.

[52] (a) G. Pacchioni and N. Rösch, *Inorg. Chem., 29* (1990) 2901; (b) N. Rösch, L. Ackermann and G. Pacchioni, *J. Am. Chem. Soc., 114* (1992) 3549.

[53] B. Spencer, A.J. Whoolery and L.F. Dahl, unpublished results.

[54] R.G. Woolley, *Inorg. Chem., 24* (1985) 3525.

[55] G. Longoni, M. Manassero and M. Sansoni, *J. Am. Chem. Soc., 102* (1980) 3243.

[56] A. Ceriotti, F. Demartin, G. Longoni, M. Manassero, M. Marchionna, G. Piva and M. Sansoni, *Angew. Chem., Int. Ed. Engl., 24* (1985) 697.

[57] D.A. Nagaki, J.V. Badding, A.M. Stacy and L.F. Dahl, *J. Am. Chem. Soc., 108* (1986) 3825.

[58] A.F. Wells, *Structural Inorganic Chemistry,* Oxford University Press, London, 5th edn., 1984, pp. 71–72.

[59] (a) R. Bouwman and W.M.H. Sachtler, *J. Catal., 19* (1970) 127; (b) R. Bouwman, G.J.M. Lippits and W.M.H. Sachtler, *J. Catal., 25* (1972) 350; (c) F.L. Williams and M. Boudart, *J. Catal., 30* (1973) 438.

[60] (a) J.H. Sinfelt, *Acc. Chem. Res., 20* (1987) 134; (b) *Sci. Am., 253* (1985) 90; (c) *Bimetallic Catalysts: Discoveries, Concepts, and Applications,* Wiley, New York, 1983, pp. 1–164, and refs. therein; (d) W.M.H. Sachtler and R.A. van Santen, *Adv. Catal., 26* (1977) 69; (e) J.H. Sinfelt, *Prog. Solid State Chem., 10* (1975) 55; (f) Bimetallic catalysts, in *Proc. Robert A. Welch Foundation Conf., Chemical Research: XXV. Heterogeneous Catalysis, Houston, TX, 1983,* Ch. V, pp. 141–176.

[61] (a) G.A. Somorjai, *Chemistry in Two Dimensions: Surfaces,* Cornell University Press, Ithaca, NY, 1981; (b) D.M.P. Mingos and L. Zhenyang, *Comments Inorg. Chem., 9* (1989) 95.

[62] G.C. Bond, *Catalysis by Metals,* Academic Press: New York, 1962.

[63] V.G. Albano, L. Grossi, G. Longoni, M. Monari, S. Mulley and A. Sironi, *J. Am. Chem. Soc., 114* (1992) 5708.

[64] G. Doyle, K.A. Eriksen and D. Van Engen, *J. Am. Chem. Soc., 107* (1985) 7914.